암석의 전단 파괴인성 측정에 관한 실험적 연구

윤정석[1], 전석원[2]

An Experimental Study on Mode II Fracture Toughness Determination of Rock

Jeoungseok Yoon and Seokwon Jeon

Abstract. This study presents a newly suggested test method of Mode II fracture toughness measurement called "Punch Through Shear Test" which was originally proposed by Backers and Stephansson in 2001. The purpose of this study is to check the validity of the suggested testing method by performing Mode II fracture toughness tests for Daejeon Granite. In addition, the optimal specimen geometry for the testing and the relation between Mode II fracture toughness and confining pressure were also investigated. Fractured surface was observed to be very smooth with lots of rock debris which came off fracture surface which obviously implies that the surface was sheared off. This confirms that Mode II fracturing actually occurred. In addition, numerical analyses including continuum analysis, particle flow code analysis and crack propagation simulations were performed. Results of these numerical analyses indicated that the cracks occurred in the specimen were predominantly in Mode II and these cracks led to failure of the test specimen. From this investigation, it can be concluded that the newly suggested "Punch Through Shear Test" method provides a reliable means of determining the Mode II fracture toughness.

KeyWords: Mode II fracture toughness, Particle flow code, Crack propagation simulation

초 록. 본 연구에서는 2001년 Backers와 Stephansson이 제안한 Punch Through Shear Test를 소개한다. 본 연구의 목적은 대전화강암을 사용하여 이 시험법이 암석의 전단 모드 파괴인성 측정법으로서의 적합성을 알아보는 것이다. 또한, 전단모드 파괴인성을 구하기 위한 최적의 시료형상을 결정하고 전단모드 파괴인성과 봉압과의 관계를 규명하였다. 시험결과, 인장 파괴에서와 같이 거친 파괴면이 형성되지 않고 전단을 받았음을 알 수 있는 부드러운 파괴면이 관찰되었다. 시료형상에 대한 연속체 해석과 입자유동 해석 그리고 균열전파 시뮬레이션을 수행한 결과 시료내부에서 일어나는 균열의 발생은 주로 전단모드이고 이러한 전단균열들로 인해 시료의 파괴가 발생함을 입증할 수 있었으며, 결과적으로 Punch Through Shear Test는 암석의 전단모드 파괴인성 측정법으로서 적합함을 입증할 수 있었다.

핵심어: 전단모드 파괴인성, 입자유동 해석, 균열전파 시뮬레이션

1. 서 론

In modelling of rock structure, we view the rock mass as consisting of rock material itself and the fractures. Fracture acts as a weakening factor when we evaluate the strength of rock structure. So we should carefully take fractures into consideration when we calculate the strength of the rock structures. This is why the concept of rock fracture mechanics has been accepted by many fields of rock engineering.

The stress intensity factor K, which is dependent on the geometry of a cracked structure, represents the strength of stress intensity of a crack tip and has dimension of stress times length$^{1/2}$. For a given cracked body with known loading configuration and magnitude, K and corresponding stresses and displacements can be determined. This implies that there exists a critical value of K, named fracture toughness, which expresses resistance to crack pro

[1]Graduate Student, School of Civil, Urban & Geosystem Eng., Seoul National University
[2]Assistant Professor, School of Civil, Urban & Geosystem Eng., Seoul National University
접수일: 2002년 12월 24일
심사 완료일: 2003년 1월 20일

pagation. Crack initiation will take place when the K exceeds its critical value, K_C. In fracture mechanics, fracture toughness is the most important parameter.

Based on the loading type that a material is subjected to, as it can be seen in figure 1, there are three basic crack propagation modes in a fracture process; Mode I (extension, opening), Mode II (shearing, sliding) and Mode III (shearing, tearing). Among the three cases of fracturing, Mode I is the most important and common. As a consequence, most works on fracture mechanics have been focused on the Mode I loading type. In real world, however, especially in fracture problems involving rock structures, Mode II and Mixed mode I & II are quite common.

However, very little experimental and theoretical work has been done on this mode of failure. In this study, pure
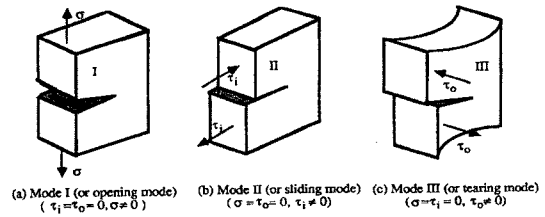
(a) Mode I (or opening mode)
($\tau_i = \tau_o = 0, \sigma \neq 0$)

(b) Mode II (or sliding mode)
($\sigma = \tau_o = 0, \tau_i \neq 0$)

(c) Mode III (or tearing mode)
($\sigma = \tau_i = 0, \tau_o \neq 0$)

Figure 1. Mode I, II and III fracturing patterns.

Mode II fracture toughness test presented by Stephansson is re-examined and how the toughness varies with confining pressure are given. In addition, the testing method is verified by numerical analyses to see if Mode II fracturing predominantly takes place in this given testing geometry. The objective of this paper on hand is to check the validity of this newly suggested testing method.
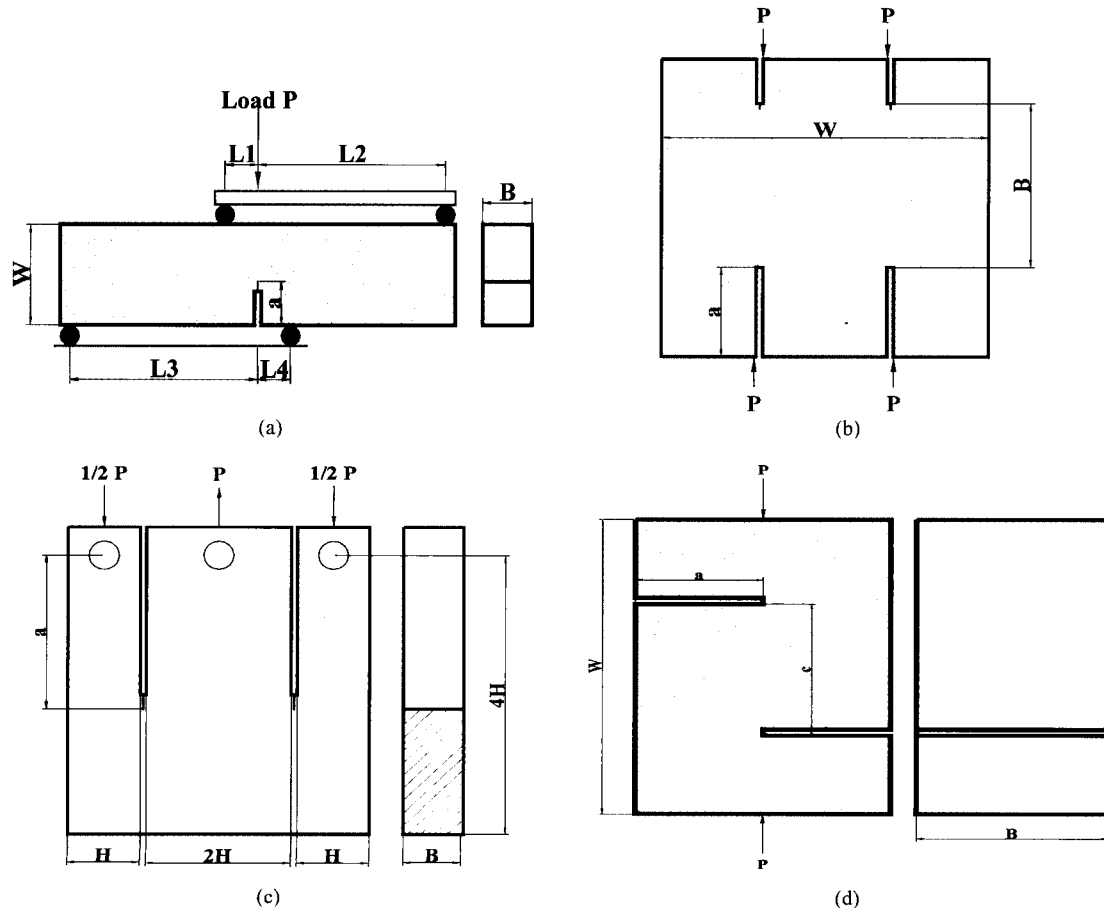
Figure 2. Mode II fracture toughness testing methods.

2. Overview of Mode II Fracture Toughness Testing Methods

Antisymmetric four point bending test was designed by Ingraffea [1] and Kim [2] to measure a Mixed Mode I & II fracture toughness (Figure 2-a). It is possible to measure pure Mode II fracture toughness under specific geometries conditions by this testing method. Punch through shear test was proposed by Wakins [3] to measure pure Mode II fracture toughness of soil-cement (Figure 2-b). Numerical (FEM) validation was done by Davies et al. [4] and it showed that failure takes place almost in Mode II. Compact double shear test specimen (Figure 2-c) was designed by Jones and Chisholm [5] to experimentally evaluate Mode II fracture toughness of aluminium. Later, it was applied to determine the Mode II fracture toughness for a variety of rocks by Laqueche et al. [6]. Short beam compression test was designed by Wakins and Liu [7] and Liu et al. [8] to determine Mode II fracture toughness of a reinforced concrete (Figure 2-d).

3. Laboratory Testing for K_{IIC}

A specimen is loaded by a Hoek cell with a confining pressure and an axial force is applied on the inner part of the sample. This leads to concentration of maximum shear stress at the upper and lower notch tip. And a zone of high shear stress is formed between the two notches from which Mode II failure is to be generated.

3.1 Testing material and sample preparation

The mechanical properties of the rock specimen used in this study are shown in Table 1. They were obtained from a series of laboratory tests on Daejeon Granite. A rock core of 52 mm in diameter is cut into pieces with length equal to the diameter. End surfaces were polished perpendicular to the lateral surface. The upper and lower

Table 1. Mechanical properties of Daejeon Granite.

Mechanical properties	Value
Uniaxial compressive strength	150±20 (MPa)
Young's modulus	58.5±7.2 (GPa)
Poisson's ratio	0.28±0.03
KIC (BDT-test)	1.18±0.12 (MPa · m$^{1/2}$)

Figure 3. Geometry of the test specimen and its dimensions.
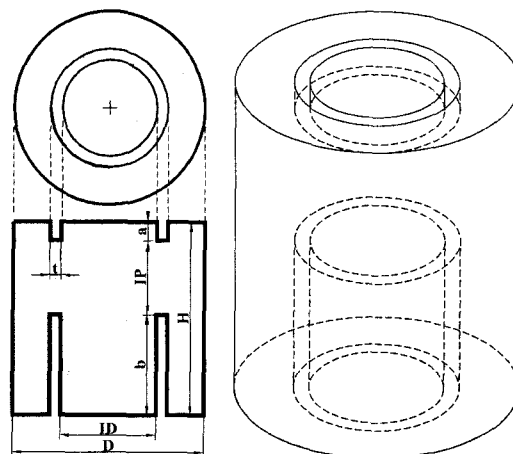
Abbre.	Description	Value (mm)
H	Sample height	52
D	Sample diameter	52
a	Upper notch depth	5
b	Lower notch depth	7, 17, 27
t	Notch width	3
ID	Inner diameter	26
IP	Intact rock portion	20, 30, 40

notches were drilled into the two end surfaces. The 5 mm deep upper notch was drilled first and then the lower notch with depth of 7, 17, 27 mm was drilled. Typical specimen geometry for the test and its dimensions are shown in figure 3.

3.2 Experimental setup

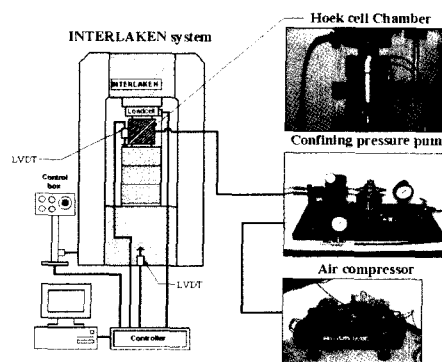Special devices for applying axial load were manufactured for this study. A stiff servo-controlled loading

Figure 4. Schematic diagram of test apparatus.

machine was used. The confining pressure was applied by SBEL Model AP-1000 pump. Compressed air was used as a power source for the pump. The output pressure regulator was attached so that the pressure inside Hoek chamber was maintained at a fixed level when the axial load was applied. The schematic diagram of the test apparatus is shown in figure 4.

3.3 Testing conditions

Table 2 shows all the testing parameters considered in this study. In this experiments, the controllable parameters were the intact portion, IP, and the confining pressure, P. Three different magnitudes P were applied in each test specimen having three different lengths of intact portion. And to eliminate typical errors caused by rock variability and preparation, three replicas were made for each test. In total twenty-seven tests were carried out.

3.4 K$_{IIC}$ determination

In our test, displacement approach proposed by Backers

Table 2. Test control parameters.

Control parameter	Fixed	Variable
Outer diameter, D	52 mm	----
Inner diameter, ID	26 mm	---
Notch width, t	3 mm	---
Upper notch depth, a	5 mm	---
Intact portion, IP	---	20, 30, 40 mm
Sample height, H	52 mm	---
Confining pressure, P	---	0, 5, 10 MPa
Loading rate	0.2 mm/min	----

and Stephansson [9] was used since only the axial deformation of the specimen was monitored during the tests. Figure 5 shows the specimen geometry near the upper notch tip. Crack tip displacement components u in the x-direction and v in the y-direction for Mode II are expressed in equations (1) and (2).

$$u = \frac{K_{II}}{4\mu} \sqrt{\frac{r}{2\pi}} \left[(2k+3) \sin \frac{\theta}{2} + \cos \frac{3\theta}{2} \right] \quad (1)$$

$$v = \frac{K_{II}}{4\mu} \sqrt{\frac{r}{2\pi}} \left[-(2k-3) \cos \frac{\theta}{2} - \cos \frac{3\theta}{2} \right] \quad (2)$$

where, k is $3-4\nu$ and $(3-4\nu)/(1+\nu)$ for plane strain and plane stress, respectively and μ is shear modulus expressed as $\mu = E/2(1+\nu)$.

In the direction of shear, where $\theta = 0$, displacement component, u is zero. Rearranging equation (2) gives:

$$K_{II} = v\sqrt{\frac{2\pi}{r}} \left[\frac{E}{4(1+\nu)(1-2\nu)} \right] \quad (3)$$

Axial force, F, causes total displacement $\Delta\delta$, which is measured by LVDT and has to be subtracted by the elastic deformation Δs occurred in the upper inner part of the specimen. The procedure mentioned above is expressed by the following equation, which leads to the actual displacement of the notch tip.

$$v = \Delta\delta - \Delta s = \Delta\delta - \left[\frac{4F}{\pi ID^2} \frac{a}{E} \right] \quad (4)$$

Plotting equation (3) with respect to the distance from the notch tip, r, gives an infinite value at the notch tip, which is practically invalid. To overcome this singularity problem, a method proposed by Chan et al. [10] was used,
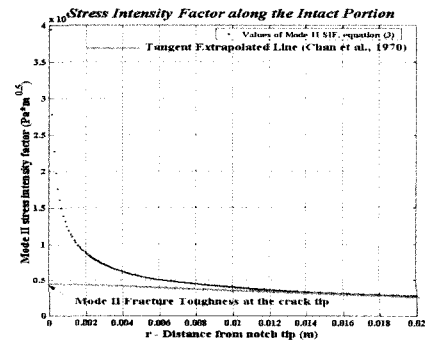

Figure 5. Geometry and nomenclatures around the upper notch tip.

Figure 6. Procedure of tangent extrapolation method.

which is to draw a tangential extrapolated line on the linear part of the curve. The point where the tangentially extrapolated line meets K_{II} axis is K_{IIC}. Figure 6 shows the above procedure.

3.5 Test results

This section presents three main categories of test results: 1) Effect of intact portion length, 2) Effect of confining pressure, and 3) Fracture patterns in the rock specimen. Table 3 shows the summarized test results. K_{IIC} was calculated with varying intact portion length from 20 to 40 mm. Values of K_{IIC} show slight fluctuation as shown in figure 7, however, they are less scattered in the range of 15~30 mm. This coincides with the results of Backers and Stephansson's [9] showing that values of K_{IIC} remain consistent when determined in the ratio of IP/W from 0.2 to 0.5. The dependency of K_{IIC} on confining pressure was examined by linear regression analysis. Figure 8 shows that K_{IIC} increases with the increase of confining pressure and they show quite linear relations between them.

Fracture patterns were observed after the tests. Similar pattern was observed through out the tests showing that fracture surface was formed between the upper inner notch tip and the lower outer notch tip. And the fracture surface is shown to be very smooth, additionally powder and dust were observed on the fracture face indicating that the surface is sheared off. Figure 9 show the fracture patterns of Daejeon Ganite specimen for 20, 30, 40 mm intact portion length. As can be seen in the figures,

fractures that connect the upper inner notch and the lower outer notch were observed in all three cases. The line of fracture surface, however, was quite straight for short intact portion length but became curved as the intact portion increased from 20 to 40 mm. The marks drawn on the figures indicate where the maximum shear stress was relatively high compared to other regions of the specimen. Therefore, cracks formed in this region can be inferred to be Mode II type cracks.

The underlined values in Table 3 are relatively high comparing with the data in literature. According to Ingraffea [1], K_{IIC} of Westerly Granite was reported to be within the range of 2.25 and 20.6. Large difference in the K_{IIC} obtained in this test and data in literature can be inferred from the notch width. Unlike in other fracture toughness test, the notch width t that was used in this test
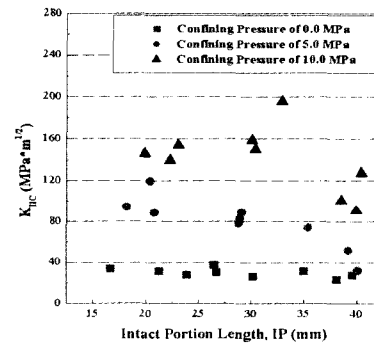

Figure 7. Relation between K_{IIC} and the length of intact portion.

Table 3. Summarized test results.

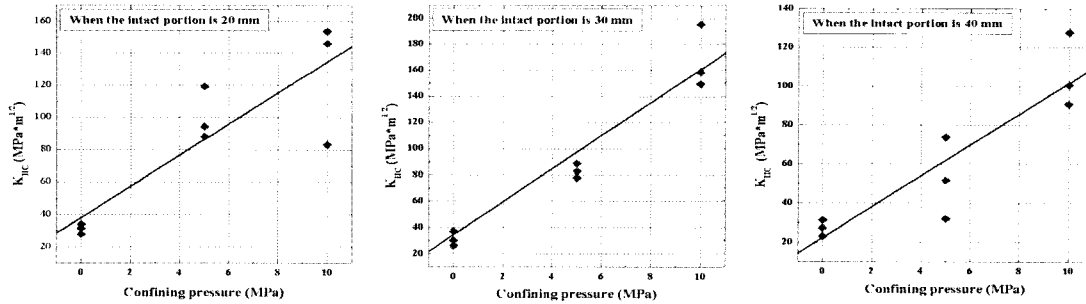| IP (mm)	Actual IP Mean/S.D. (mm)	Mode II fracture toughness (MPa · m$^{1/2}$)		
		$\sigma_c^* = 0$ MPa	$\sigma_c = 5$ MPa	$\sigma_c = 10$ MPa
20	20.79/2.29	27.93	119.22	153.64
		31.39	88.25	145.76
		33.90	94.27	83.09
30	29.26/1.80	26.20	82.83	149.64
		37.33	88.95	158.67
		30.20	77.80	195.63
40	38.46/1.99	31.48	32.01	90.72
		27.49	51.71	127.07
		23.11	73.77	100.61

σ_c^* = confining pressure

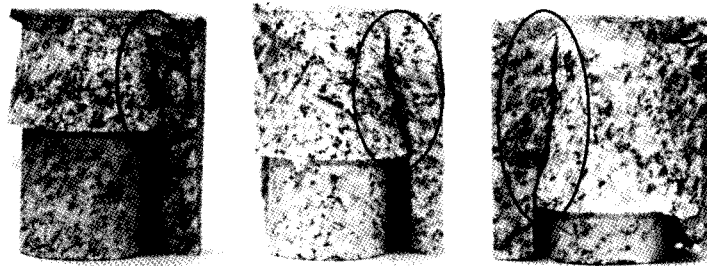**Figure 8.** Relation between K_{IIC} and the confining pressure.

Figure 9. Fracture patterns of Daejeon Granite by Punch through shear test.

method was relatively large which is possibly caused by the drill bit tip thickness.[1] Blunt notch leads to less notch effect (stress concentration) and produces non-planar fracture surface and finally results in high value of K_{IIC}. The obtained K_{IIC} shows scattering and the reason for this scattering can be explained as follows: 1) The tested rock material was somewhat heterogeneous, which means that rock cores were drilled from different boreholes, 2) Perfect configuration of sample geometry could not be achieved due to errors during the sample preparation.

4. Numerical Analysis

4.1 Continuum analysis

Axis symmetric two-dimensional finite element analysis was carried out by FRANC2D code to investigate the stress distribution in the specimen. Figure 10 presents the geometry, loading and boundary conditions for FEM analysis. Parameters were identical with those values shown in figure 3. Figure 10-a, b and c present contour

plots of maximum principal stress, σ_1, minimum principal stress, σ_2 and maximum shear stress, τ_{MAX}, when the specimen is under 100 MPa of axial load with the confinement of 5 MPa, which is the typical loading configuration in this test. As shown in the figure, τ_{MAX} was concentrated at the upper inner and lower outer notch tip and from the stress contour it can be seen that the maximum shear stress is more or less parallel to the plane between the notches. The maximum shear stress τ_{MAX}, generates initiation of shear crack and leads to shear failure of the plane between the upper and lower notch which is the desired failure mode. On the opposite side of the notch tips where τ_{MAX} is highest, concentration of tensile stress is generated. Figure 11-d, e show the tensile and compressive stress flow in the specimen by displaying vectors of principal stresses at each gauss point. As the figures indicate, concentration of tensile stress is generated at the upper outer and lower inner notch and these tensile stresses caused a Mode I crack initiation.

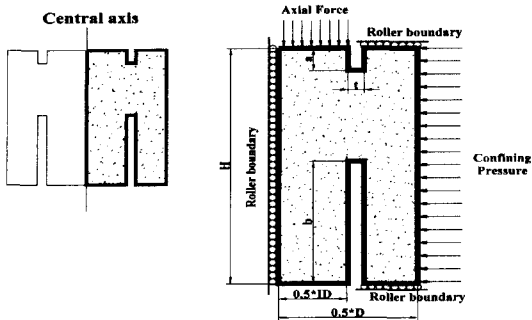1) ISRM suggested test method: notch width ≤ the greatest of 0.03D and 1 mm, where D is specimen diameter.

Figure 10. Geometry, loading and boundary conditions for finite element analysis.

4.2 Particle flow analysis by PFC^{2D}

Particle flow model simulations were performed. In this model, the continuum behavior was approximated by treating the solid as a compacted assembly of many small particles. For the simulation of the real triaxial PTS test, throughout the loading process, the confining pressure was kept constant by adjusting the lateral-wall velocities using a numerical servo-mechanism. The sample was loaded in a strain-controlled condition by specifying the velocities of the top and bottom walls. Table 4 presents the inputs that control the specimen-genesis procedure and that define the PFC^{2D} material. The material strengths are picked from a Gaussian (normal) distribution and are specified in terms of a mean and a standard deviation. The formations of damage in the specimen is shown in figure 12. The result of the numerical analysis was satisfactory when compared with the laboratory test results. Cracks formed in the elliptical region marked on the figure are shear type, where as wing shaped crack patterns are mainly composed of normal breakages of bond between particles. As seen in the figure, large

    (a)   (b)   (c)

    (d)   (e)
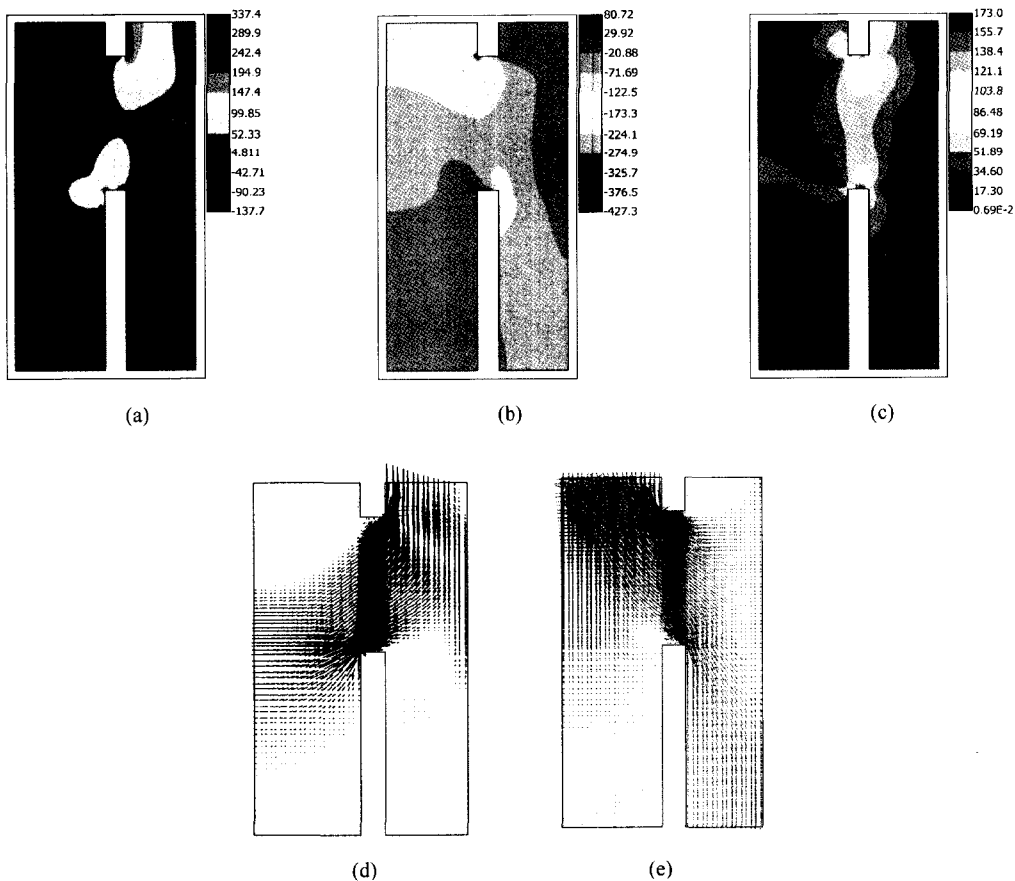
Figure 11. Contour plots of σ_1, σ_2, τ_{MAX}, tensile and compressive stress flow in the specimen.

Table 4. Inputs to the PFC^{2D} analysis.

Parameter	Description	Value
Parameters that control the specimen-genesis procedure		
h	sample height [m]	0.052
w	sample width [m]	0.052
R_{min}	minimum ball radius [m]	0.0002
R_{max} / R_{min}	ball size ratio, uniform distribution	1.66
Microparameters that define a contact-bonded material		
ρ	ball density [kg/m³]	3170
E_c	ball to ball contact modulus [GPa]	103
k_n / k_s	ball stiffness ratio	3.4
μ	ball friction coefficient	0.25
σ_c	contact-bond normal strength, mean [MPa]	110
σ_c	contact-bond normal strength, std. dev. [MPa]	0
τ_c	contact-bond shear strength, mean [MPa]	220
τ_c	contact-bond shear strength. std. dev. [MPa]	0

number of shear cracks are generated in the specimens of 20 mm intact portion compared to the specimen of 30 and 40 mm intact portion. Figure 13 presents a stress-strain curve of PFC^{2D} simulation for the PTS test when the intact portion and confining pressure are 20 mm and 0.1 MPa, respectively. Figure 13 shows step-by-step damage formations in the specimen during the entire loading process. Figure 14 shows dissipated energy in the specimen which is due to frictional slip (shearing of particles) and kinetic energy release resulting from the bond breakages (shear cracks). From figure 14, one can notice that the frictional energy rapidly increases at the inflection point. This is where the specimen is subjected to peak stress (strain of 0.004). This means that from the stage 4, large amount of energy is dissipated and released
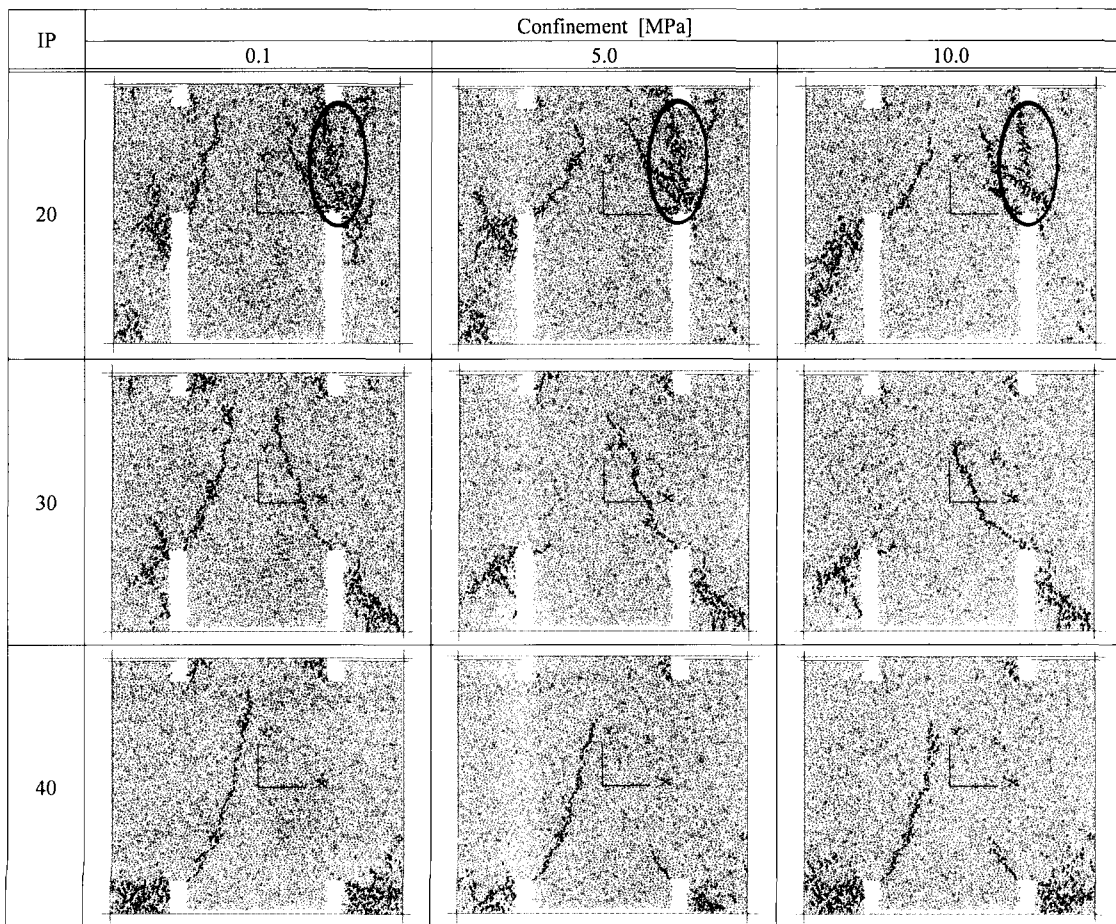

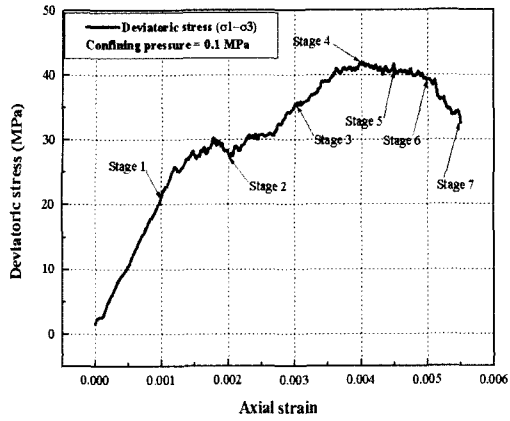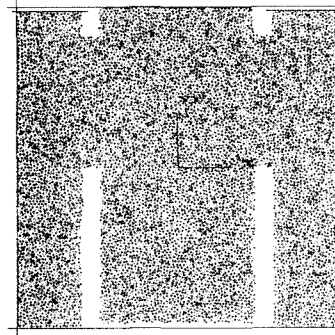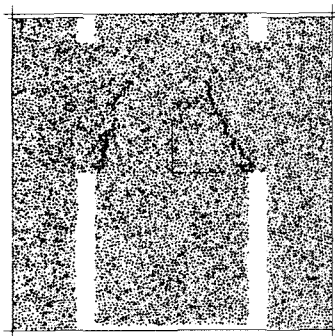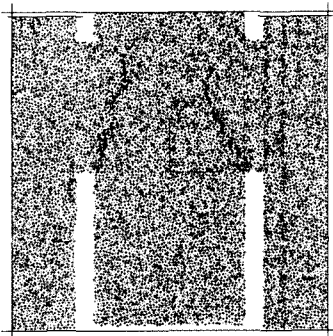**Figure 12.** Damage formations in the specimens.

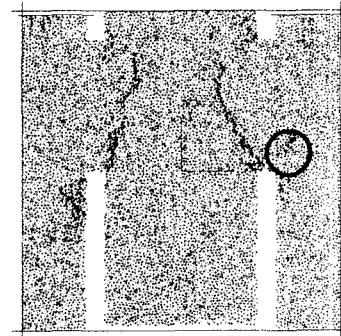Figure 13. Curve of deviatoric stress versus axial strain.
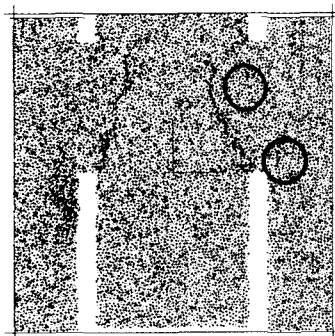
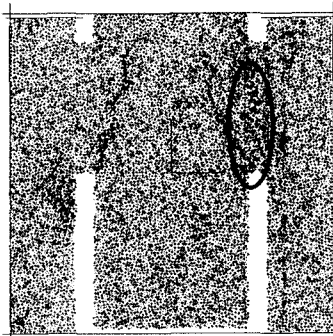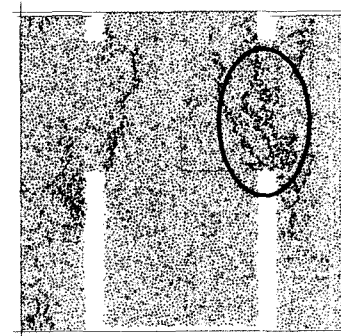Stage 1, pre-peak

Stage 2, pre-peak

Stage 3, pre-peak

Stage 4, peak

Stage 5, post-peak

Stage 6, post-peak

Stage 7, failure

Figure 14. Microcracks in the specimens.

by shearing of particles and by shear-type bond breakages. Damage formations at stage 4, 5, 6, 7 in figure 13 well demonstrate above statement and lead to conclusion that shear-type cracks generated from stage 4 finally leads to the shear failure of the specimen.

4.3 Crack propagation simulation

Crack propagation simulation was carried out on the test specimen. The main purpose if this simulation was to examine whether cracks initiated between the upper inner notch and the lower outer notch were truly shear type. The specimen having 20 mm of intact portion was
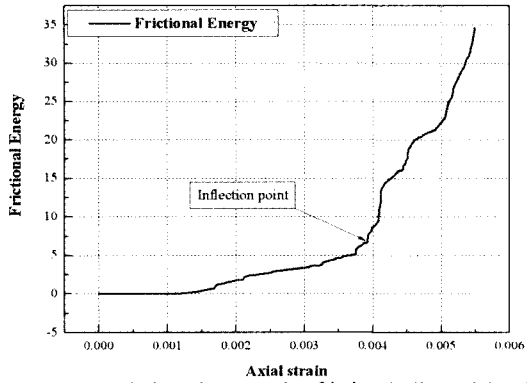
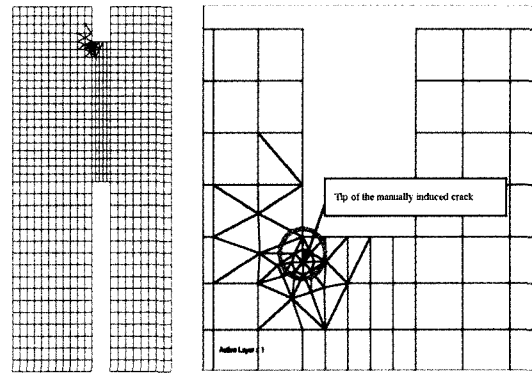Figure 15. Dissipated energy by frictional slip and bond breakages.

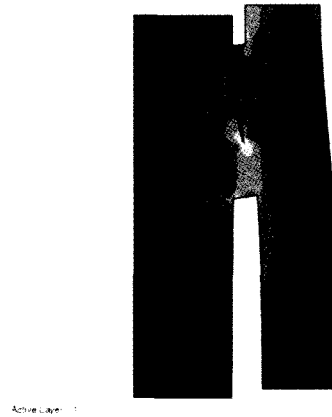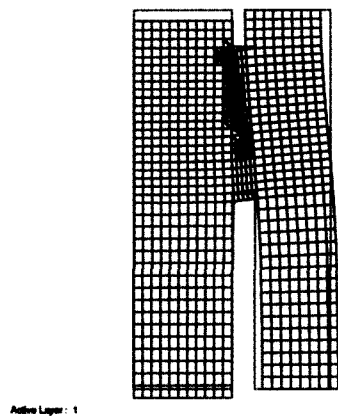Figure 16. Crack initiation at the upper notch.

Figure 17. Deformed shape of the specimen and the distribution of the maximum shear stress.
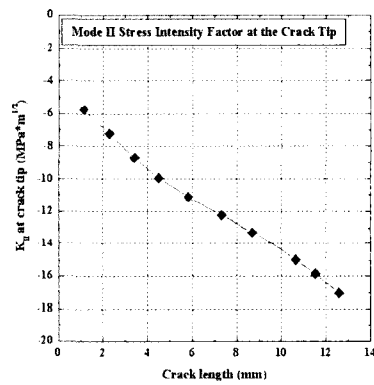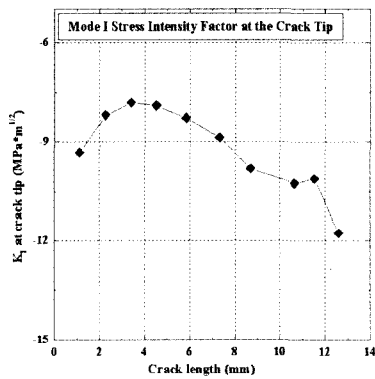

Figure 18. History plot of Mode I and II stress intensity factors with respect to crack length.

investigated since the fracture pattern was quite obvious and similar as can be seen in figure 8 and 11. Crack was initially put in the specimen, as shown in figure 15, where the concentration of the maximum shear stress appeared.

Figure 16 shows the finally deformed shape and stress distribution of the specimen. Stress intensity factors were calculated along the crack tip as it propagated and they are shown in figure 17. Negatives values of K_I and K_{II}

at the crack tip physically imply that the crack tip and plane are subjected to shearing under compression. These phenomena were observed in the tested specimens. The fractured surface was shown to be smooth and rock powder and dust were observed which obviously infers that the surface was sheared off.

5. Conclusions

From this study, following conclusions can be drawn.
1. The validity of the newly suggested K_{IIC} test method was proved.
2. Proper geometry of the test specimen was determined: Diameter = 52 mm, Height = 52 mm, upper inner notch depth = 5 mm, lower notch depth = 17~32 mm and inner cylinder diameter = 26 mm.
3. Relation between K_{IIC} and confining pressure was investigated by linear regression analyses and it was found that the K_{IIC} increases with increasing confining pressure.
4. The failure of the specimen was mostly due to the shear mode fracturing, partly accompanied by tensile mode.
5. Fractured surface occurred connecting the upper inner notch tip and the lower outer notch tip.
6. Sheared surface was formed between two notches and it can be inferred that Mode II cracks occurred along the fracture surface.
7. Fractured surface shows a very smooth surface which obviously implies that surface is sheared off.
8. Numerical continuum analyses reveal that maximum shear stress is concentrated at the upper inner notch tip and lower outer notch tip. Cracks occurred in this region of high shear stress are predominantly in Mode II. This result was verified by particle flow model and crack propagation simulation.
9. From the above results, we can conclude that Mode II failure predominantly occurred in the test specimen and this suggested method provides a reliable means of determining Mode II fracture toughness.

Acknowledgements

References

1. Ingraffea, A.R. 1981. Mixed-Mode fracture initiation in India limestone and Westerly granite. Einstein, H.H. (ed.), Proceedings 22nd U.S. Symposium. Rock Mech.: 199-204. MIT: Cambridge.
2. Jae-Dong Kim, Chung-In Lee, 1988, A study on the Measurement of Fracture Toughness and Fracture Propagation in Rock, Ph.D. Dissertation, Graduate school of Seoul National University.
3. Wakins, J. 1983. Fracture toughness test for soil-cement samples in Mode II. International Journal of Fracture 23: R135-138.
4. Davies, J. & Morgan, T.G. & Yim, A.W. 1985. The finite element analysis of a punch-through shear specimen in mode II. International Journal of Fracture 28: R3-10.
5. Jones, D.J. & Chisholm, D.B. 1975. An investigation of the edge-sliding mode in fracture mechanics. Engineering Fracture Mechanics 7: 261-270.
6. Laqueche, H. & Rousseau, A. & Valentine, G. 1986. Crack propagation under mode I and mode II loading in slate schist. International Journal of Rock Mechanics and Mining Science & Geomechanics Abstract 23 (5): 347-354.
7. Wakins, J. & Liu, K.L.W. 1985. A finite element study of the short beam test specimen under mode II loading. International Journal of Cement Composites and Lightweight Concrete 7: 93-101.
8. Liu, K. & Barrt, B.I.G. & Wakins, J. 1985. Mode II fracture of fiber reinforced concrete materials. International Journal of Cement Composites and Lightweight Concrete 7: 93-101.
9. Backers, T., Stephansson, O. 2001. Punch-through shear test of drill core - a new method for KIIC testing. Diploma thesis, Division of Engineering Geology, Technical University Berlin, Germany.
10. Chan, S.K. & Tuba, I.S. & Wilson, W.K. 1970. On the finite element method in linear fracture mechanics. Engineering Fracture Mechanics 2: 1-17.
11. Soo-Ho Chang, Chung-In Lee, 1999, A study on the Measurement of Rock Fracture Toughness under Mode I, II & Mixed Mode, Tunnel and Underground Space, Korean Society for Rock Mechanics, Vol. 9, No. 4, 315-327.
12. Personal communication with Ove Stephansson, Eurock 2001, Espoo, Finland
13. T. Backers, O. Stephansson and E. Rybacki, 2002, Rock fracture toughness testing in Mode II - punch-through shear test, International Journal of Rock Mechanics and Mining Sciences 39, 755-769.
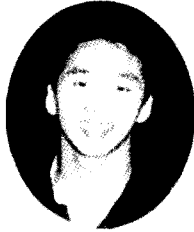
윤 정 석

2000년 한동대학교 공과대학 건설도시환
경공학부 공학사
2002년 서울대학교 지구환경시스템공학
부 공학석사

Tel: 02-880-7230
E-mail: joshyoon@rockeng.snu.ac.kr
현재 서울대학교 지구환경시스템공학부
박사과정

전 석 원

1987년 서울대학교 공과대학 자원공학
과 공학사
1989년 서울대학교 대학원 자원공학과
공학석사
1991년 미국 캘리포니아 주립대학 공학
석사
1991년 미국 아리조나 주립대학 공학박사
Tel: 02-880-8807
E-mail: sjeon@rockeng.snu.ac.kr
현재 서울대학교 지구환경시스템공학부
조교수